International Journal of Coal Geology 223 (2020) 103450

Contents lists available at ScienceDirect

International Journal of Coal Geology

journal homepage: www.elsevier.com/locate/coal

Experimental observations of heterogeneous strains inside a dual porosity sample under the influence of gas-sorption: A case study of fractured coal

Rui Shi[a,b,d], Jishan Liu[c], Xiaoming Wang[a,*], Derek Elsworth[d], Zhanghao Liu[e], Mingyao Wei[f], Xingxing Liu[g], Zhizhuang Wang[a]

[a] Key Laboratory of Tectonics and Petroleum Resources, Ministry of Education, China University of Geosciences, Wuhan 430074, China
[b] School of Energy and Mining Engineering, China University of Mining and Technology, Beijing 100083, China
[c] Department of Chemical Engineering, School of Engineering, The University of Western Australia, 35 Stirling Highway, WA 6009, Australia
[d] Department of Energy and Mineral Engineering, G3 Centre and Energy Institute, The Pennsylvania State University, University park, PA 16802, USA
[e] State Key Laboratory of Geomechanics and Geotechnical Engineering, Institute of Rock and Soil Mechanics, Chinese Academy of Sciences, Wuhan 430071, China
[f] IoT Perception Mine Research Center, China University of Mining & Technology, Xuzhou 221116, China
[g] College of Water Conservancy and Hydropower Engineering, Hohai University, Nanjing 210098, China

ARTICLE INFO

Keywords:
Dual porosity
Stress transfer
Swelling strain
Non-equilibrium deformation
Sorption-induced swelling/shrinking

ABSTRACT

A "permeability equilibration time" is typically assumed in interpreting permeability measurements – indicating that equilibration has been reached and both sorption-induced changes in deformation and their impact on permeability evolution have ceased. However, for extremely low matrix permeability (tight) dual porosity rocks, this "permeability equilibration time" may easily exceed the time interval between two consecutive permeability measurements – invalidating the interpretation of a steady permeability if the non-steady state conditions are not correctly accommodated. This is especially important where pressure diffusion from fracture to matrix results in a non-monotonic and non-asymptotic approach to a steady permeability, but instead contains multiple stages, plateaus and permeability reversals. We validated this hypothesis through experiments and analysis. Experiments measured the non-monotonic and scale-dependent deformations of fracture and matrix and linked these directly to the dynamic evolution of reservoir permeability. These laboratory strain measurements were integrated with numerical analyses to explore how mass and stresses transferred between matrix and fracture and were coupled under conditions of constant confining pressure. Strain gauges were distributed to directly measure stress transfer between matrix and fracture and interrogated deformation at different scales and at different proximities to control fractures. The prismatic sample of coal was tested under freely expanding boundary conditions. Optical microscopy and X-ray CT imaging were used to define the fracture distribution throughout the sample with mercury intrusion (capillary) porosimetry (MICP) constraining the pore size distribution and enabling independent estimation of matrix permeability. A numerical model was built and verified by matching measured strains and then applying this to model the evolution coal permeability from initial to ultimate equilibrium. Both the experimental and numerical results show that the final equilibrium state (pressure, stress and mass contents) for the matrix system extends to months rather than hours and suggests that some current permeability data may therefore reflect a non-equilibrium permeability state. Results also show that during this non-equilibrium condition, the swelling of the matrix near the fracture will cause not only compaction and narrowing of the fracture, but also shrinkage of the matrix that is distant from the fracture under constant confining pressure condition. Both experimental and numerical results demonstrate that the evolution of non-equilibrium strain/permeability is determined by the matrix-fracture interactions, including sorption-induced swelling/shrinking, through transient stresses in matrix and fractures. And that these non-equilibrium stress transfers determine the dynamic permeability evolution during gas extraction (e.g., CH_4) or injection (e.g., CO_2) at reservoir scale for tight dual porosity rocks (e.g., coal and shale).

* Corresponding author.
E-mail addresses: jishan.liu@uwa.edu.au (J. Liu), sunwxm@cug.edu.cn (X. Wang).

https://doi.org/10.1016/j.coal.2020.103450
Received 19 December 2019; Received in revised form 15 March 2020; Accepted 17 March 2020
Available online 21 March 2020

List of Symbols

b_0	Initial fracture aperture (m)
Δb	Fracture aperture change (m)
f_i	The component of body force in the i –direction (N)
G	Shear modulus (MPa)
E	Young's modulus (MPa)
K	Bulk modulus (MPa)
k_m	The permeability of matrix system (m^2)
k_f	The permeability of fracture system (m^2)
k_{f0}	The initial fracture permeability (m^2)
M	The molecular mass of gas (kg/mol)
p_m	The gas pressure in the matrix systems (MPa)
p_f	The gas pressure in the fracture systems (MPa)
p_L	Langmuir pressure (MPa)
p	Pore pressure (MPa)
R	The universal gas constant (J/(mol·K))
T	The absolute gas temperature (K)
u_i	The component of displacement in the i-direction (m)
V_L	Langmuir volume constant (m^3/kg)
Q_S	Gas source or sink (kg/(m^3·s))
ϕ_m	The porosity of matrix system
ε_L	Langmuir volumetric strain constant
ν	Possion's ratio
α	Biot's coefficient
ρ_s	Coal density (kg/m^3)
ρ_a	Gas density at atmospheric pressure (kg/m^3)
ρ_g	Gas density (kg/m^3)
μ	Dynamic viscosity of the gas (mPa·s)

1. Introduction

The boom in unconventional resources (e.g., coalbed methane, shale gas) has substantially reshaped the oil and gas industry over the past two decades. Exploitation of coalbed methane (CBM) from coal seams also benefits mining safety and reduces greenhouse gas emissions (Karacan et al., 2011). Coal and shale reservoirs are generally regarded as dual porosity media that consists of the porous matrix and the surrounding fractures. However, gas adsorption/desorption induces swelling/shrinking of the matrix system (Karacan, 2007; Kiyama et al., 2011; Pan and Connell, 2007), further affecting the permeability evolution. The contrasting permeabilities of the adjoining matrix and fracture systems sustain a pressure difference between the matrix system and fracture system, together with a differential effective stress during non-equilibrium periods of gas extraction/injection. Meanwhile, interaction between matrix and fracture determines the dynamic change of reservoir permeability in dual porosity rocks and exerts a control on gas production during the drainage process (Cui et al., 2018a; Liu et al., 2017; Wang et al., 2016; Wei et al., 2019c). Thus, it is vital to understand modes of stress transfer between matrix and fracture in response to gas flow in dual porosity rocks for geoengineering activities (e.g., coalbed methane production, shale gas extraction).

Coal reservoirs can be represented as a dual porosity/permeability system. The fractures are the primary pathway for rapid fluid flow, while the coal matrix serves as a storage site with gas stored in the various-sized pores (Haenel, 1992; Zheng et al., 2018). It is commonly assumed that Darcy flow predominates in the fracture system but can be neglected in the coal matrix where diffusion dominates (Cui et al., 2018b; Fan et al., 2019; Liu et al., 2019; Palmer, 2009; Pan and Connell, 2012; Purl et al., 1991; Ried et al., 1992; Zhang et al., 2019) – although there are equivalencies between permeability and diffusivity. When gas is injected into coal, gas rapidly invades the fractures due to the relatively high permeability. As a consequence, a pressure difference between the matrix and the fracture is created and this in turn results in the diffusion of gas from the fracture into the matrix. The gas diffuses rapidly from the fractures into the matrix where there is a high matrix permeability/diffusivity (e.g., sandstone) – and the interval time for pressures to stabilize can be neglected (Shi et al., 2018). However, for coal, this may take several days (Harpalani and Chen, 1997) or even several weeks (Gensterblum et al., 2014). When, in addition to diffusion-only, the retarding impact of gas sorption is included, the time for equilibration may extend to a few months (Danesh et al., 2017; Guo et al., 2007). These coupled diffusion/sorption phenomena determine the localized deformation within the ensemble matrix-fracture system and can be investigated through tightly constrained laboratory experiments and numerical models.

Single porosity/permeability models (Connell et al., 2010; Cui and Bustin, 2005; McKee et al., 1988; Palmer and Mansoori, 1996; Pan and Connell, 2007; Pini et al., 2009; Robertson and Christiansen, 2006; Seidle et al., 1992; Seidle and Huitt, 1995; Shi and Durucan, 2004) are used under specific conditions (such as uniaxial strain) to explain the experimental observations. However, these models are not applicable in interpreting some experimental observations (Izadi et al., 2011; Liu et al., 2011b; Wang et al., 2011). On the basis of dual poroelasticity theory, dual porosity and dual permeability models have been established (Bai et al., 1993; Lu and Connell, 2007, 2011; Pan and Connell, 2007; Peng et al., 2014; Wang et al., 2013; Wu et al., 2011; Wu et al., 2010), which are capable of accommodating the roles of fracture-matrix interaction. Among these models, the interactions between coal matrix and fractures are normally defined by the mass exchange of gas. However, the role of mechanical interaction between matrix and fracture, that can cause the transition of coal matrix swelling, from local swelling to macro-swelling, under differential pressure, together with their impact on the evolution of permeability is not rigorously accommodated (Liu et al., 2011a; Liu et al., 2011b). To address this shortcoming, permeability models have been established with the interaction between matrix and fracture geometry and location suitably accommodated (Liu et al., 2018; Wei et al., 2019a; Zhang et al., 2018). In this, a full set of cross-coupling relations are connected between the matrix and the fracture, including local force balance, local deformation compatibility, and mass exchange (Zhang et al., 2018). The fracture aperture change in coal containing discrete fractures, following gas injection under unconstrained conditions, is consequently rigorously accommodated (Liu et al., 2018). This includes consideration of the non-uniform deformation induced by gas diffusion and described by a strain-rate-based permeability model coupling coal deformation and gas flows in both fractures and matrix (Wei et al., 2019a).

The majority of experimental studies on cleat-matrix interaction

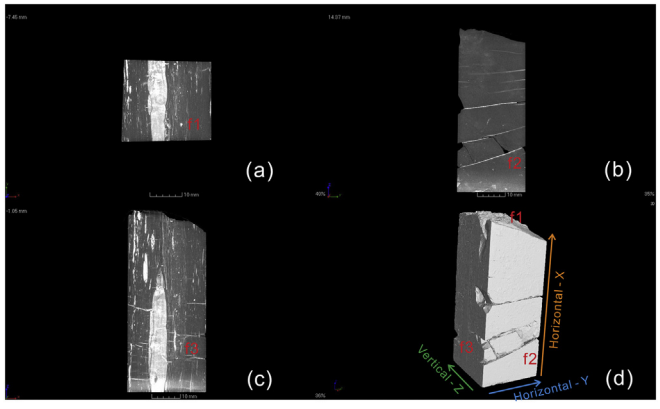

Fig. 1. CT images of the coal sample for faces: (a) f1, (b) f2, and (c) f3, (d) together with a three-dimensional view of the coal sample.

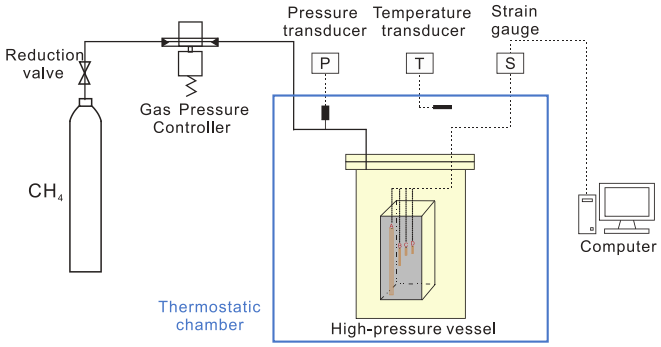

Fig. 2. Schematic of the experimental set-up to measure the sorption-induced strain.

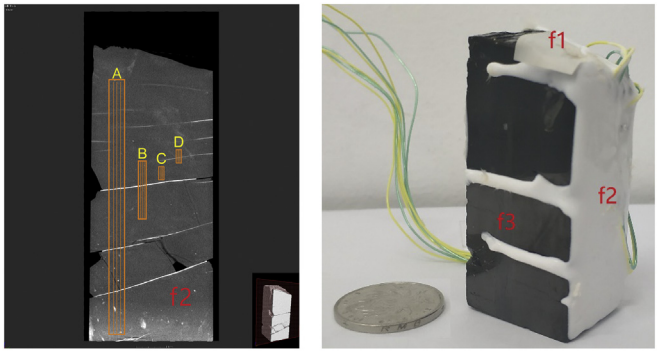

(a) CT imaging (b) Coal sample

Fig. 3. Schematic and photograph of the sample with strain gauge arrangement.

have been completed by measuring the correlation between coal permeability and pore pressure – with these experiments divided between displacement-controlled and stress-controlled experiments. For displacement-controlled experiments, uniaxial strain experiments are normally used to study the evolution of coal permeability (Fan and Liu, 2018; Mitra et al., 2012; Wang et al., 2015). As for the stress-controlled experiments, two types of experiments are generally conducted, with one keeping total stress constant (Gensterblum et al., 2014; Harpalani and Schraufnagel, 1989, 1990; Harpalani and Zhao, 1989; Kumar et al., 2012; Meng et al., 2015; Pini et al., 2009; Robertson and Christiansen, 2005; Wang et al., 2017b; Wang et al., 2019; Wang et al., 2015), and the other keeping effective stress constant (Al-hawaree, 1999; Anggara et al., 2016; Chen et al., 2011; Feng et al., 2017; Harpalani and Chen, 1997; Li et al., 2015; Li et al., 2013; Lin and Kovscek, 2014; Lin et al., 2008; Meng and Li, 2017; Pan et al., 2010; Seomoon et al., 2015; Xu et al., 2013). Regardless of the choice of boundary conditions, these experiments typically ignore the pressure difference between the matrix and the fracture – and assumes steady condition to interpret the results. In order to study the impact of dynamic deformation between matrix and fracture within the coal sample, a set of experiments have been performed to measure the evolution of dynamic permeability during gas injection/depletion under constant confining pressures (Liu et al., 2016a; Mazumder and Wolf, 2008; Siriwardane et al., 2009; Wei et al., 2019b). Importantly, the evolution of the *distribution* of strains throughout the entire samples and under different stress conditions were also observed. Helium gas (He) was injected into both jacketed and unjacketed coal samples within a pressurized core holder to investigate coal matrix swelling during the process of gas diffusion from cleats, and the impact on the evolution of strain within the entire sample were observed (Wang et al., 2016). For a constant volume boundary condition (zero displacement), local deformation of the coal sample and its permeability were measured through strain gauges and unsteady flow during helium gas injection (Wang et al., 2017a), respectively. These results demonstrated that gas diffusion from the fracture to the matrix can result in localized swelling of the coal matrix and affect the aperture of the cleat. Under this condition, coal permeability is controlled primarily by the local deformation. Normally it is assumed that 100% of the coal swelling would contribute to the reduction of coal permeability provided that the fractures are much more compliant than the coal matrix (Harpalani and Chen, 1995; Liu et al., 2011b; Ma et al., 2011). However, few direct observations of this have been made, and the distribution of deformations in different parts of the sample has not been clearly explained.

The following study observed the stress transfer between matrix and fracture through the proxy of measured strains. Strain gauges were used to measure the mean strain on different parts of a prismatic coal sample containing a variable density distribution of fractures. The sample was tested under conditions of free expansion (zero stress). Optical microscopy and X-ray CT imaging were used to define the fracture distribution throughout the sample with mercury intrusion (capillary) porosimetry (MICP) constraining the pore size distribution measured and enabling independent estimation of matrix permeability. This work offers a first direct observation into the dynamics of stress transfer between fracture and matrix and a new understanding of permeability evolution in response to the transition in dual porosity rocks. These results and findings are reported in the following sections.

2. Experimental method

Methane was sorbed into a freely swelling prismatic sample of coal sample to measure the dynamic evolution of strain at the decimeter scale. Optical microscopy and X-ray CT imaging were utilized to define the fracture distribution throughout the sample with pre-sorption porosity determined by mercury injection capillary pressure porosimetry (MICP). Surface mounted strain gauges were attached to the sample to monitor the local linear strains of different parts of the sample and at different scales, both adjacent to fractures and in the intact portion of the sample. The sample preparation and experimental techniques are introduced in the following.

2.1. Sample information

Samples of anthracite from the Qinshui Basin were used in the experiments with basic information obtained from the Optical microscopy, X-ray CT imaging and MICP tests.

2.1.1. Sample preparation

Prismatic blocks of anthracite for the deformation tests were collected from an underground coal mine in Permian-Carboniferous strata of the Qinshui Basin, China. A single prismatic sample was cut from the coal blocks, as shown in Fig. 1 (d). The height of the sample is ~5 cm with length and width of ~2 cm. The sample was dried at 50 °C for 48 h to remove moisture.

2.1.2. Optical microscopy and X-ray CT imaging

The fracture distribution on the polished faces was recorded under reflected light using an optical microscopy (Nikon, manufactured in Tokyo, Japan). X-ray computed tomography (CT) was utilized as a non-destructive technique to provide quantitative detection of the interior 3D structure of the sample (Wang et al., 2019; Wildenschild and Sheppard, 2013). In this study, the sample was scanned with a Nanotom X-ray Computed Tomography instrument (GE Phoenix) with a resolution of 1 μm.

2.1.3. Mercury injection capillary pressure porosimetry (MICP)

The geometric characteristic of the porosity distribution and connectedness determines the diffusion coefficient of the coal (Yang and

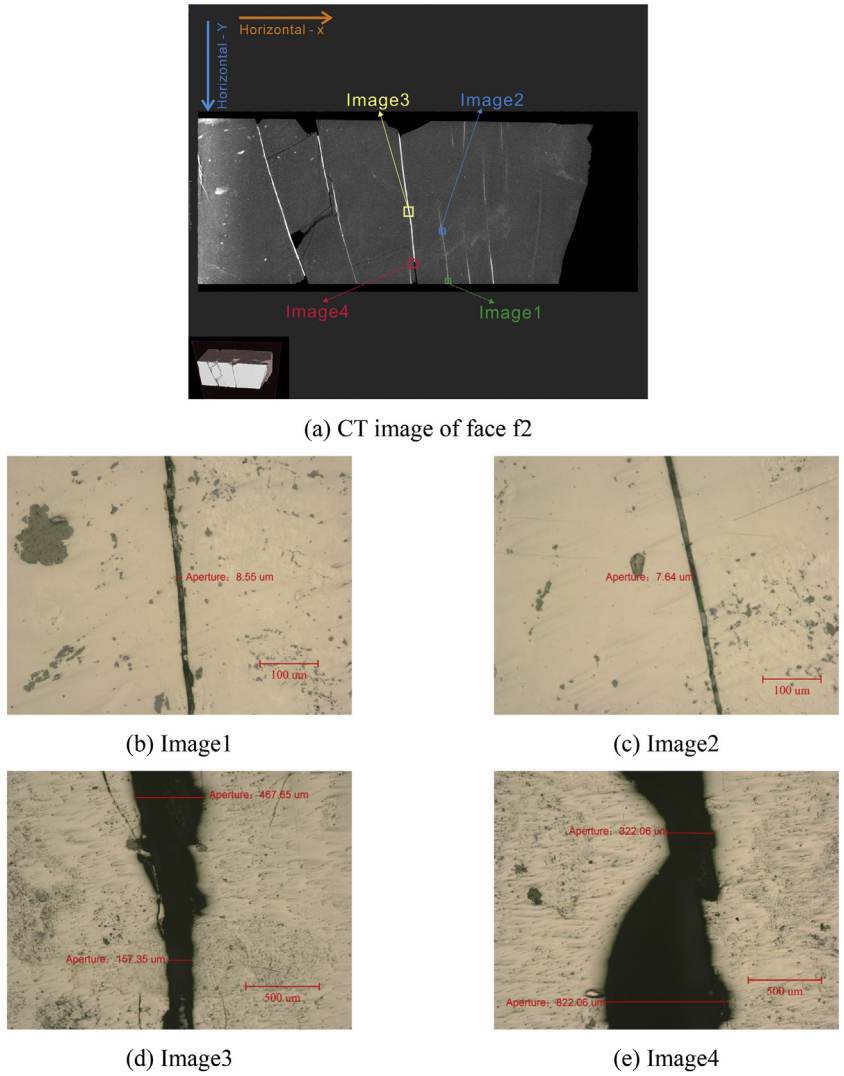

(a) CT image of face f2

(b) Image1

(c) Image2

(d) Image3

(e) Image4

Fig. 4. Fracture distribution and fracture aperture distribution on the surface of coal sample face f2 as recovered through CT imaging (a) and optical microscopy (b-e).

Liu, 2019; Zhao et al., 2019), and also affects the matrix permeability. MICP was conducted with a Mercury Injection Porosimeter (instrument: Micromeritics AutoPore IV9510) to investigate the pore size distribution of the coal sample, performed on cubic samples ~1 × 1 × 1 cm^3 after drying at 60 °C for 48 h to remove moisture (Yang et al., 2017). The surface tension of the mercury is 485 mN/m with a contact angle of 130° (Gan et al., 1972; Sun et al., 2017). The corresponding pore-throat distribution was calculated using the Washburn equation (Washburn, 1921).

2.2. Experimental set-up

The experimental set-up for this study was designed to enable the measurement of strain induced by the mechanical compression and shrinkage or swelling resulting from the gas adsorption (Liu and Harpalani, 2013). A schematic of the experimental set-up is illustrated in Fig. 2. The set-up comprises a gas pressure controller, pressure monitoring system, high-pressure vessel and a data acquisition system to monitor the strains. The vessel was placed in a thermostatic chamber to eliminate the thermal impact on the deformation of the coal sample.

2.3. Experimental procedure

Strain gauges were applied to the sample to measure the spatial distribution of coal deformation history, and to resolve the coupling between shrinkage deformation and dynamic gas injection (Kiyama et al., 2011; Liu et al., 2016b). The experimental set-up using strain gauges was designed and employed to measure the sorption-induced strain in the horizontal direction (Liu and Harpalani, 2013; Sang et al., 2017). Four strain gauges were installed on the designated surface of the sample so as to monitor the local linear strains in the horizontal direction (Fig. 3a). According to the distribution of natural fractures, Gauge A was used to measure the average deformation of the whole sample; Gauge B was adopted to measure the average deformation of the part of the sample that crosses a single dominant (large) fracture; Gauge C was arranged to measure the average matrix deformation of one part of the sample that contains no fractures, and; Gauge D was used to measure the average deformation of one part of the sample that crosses a small fracture, as shown in Fig. 3 (a). After the attachment of gauges, the instrumented surface (f2) was covered in soft silicone rubber adhesive to protect the strain gauges for the long-time deformation test and to prevent gas from entering the sample across this surface, as shown in Fig. 3 (b). The entire assembly was then placed in the pressure vessel, as illustrated in Fig. 2. After thermally

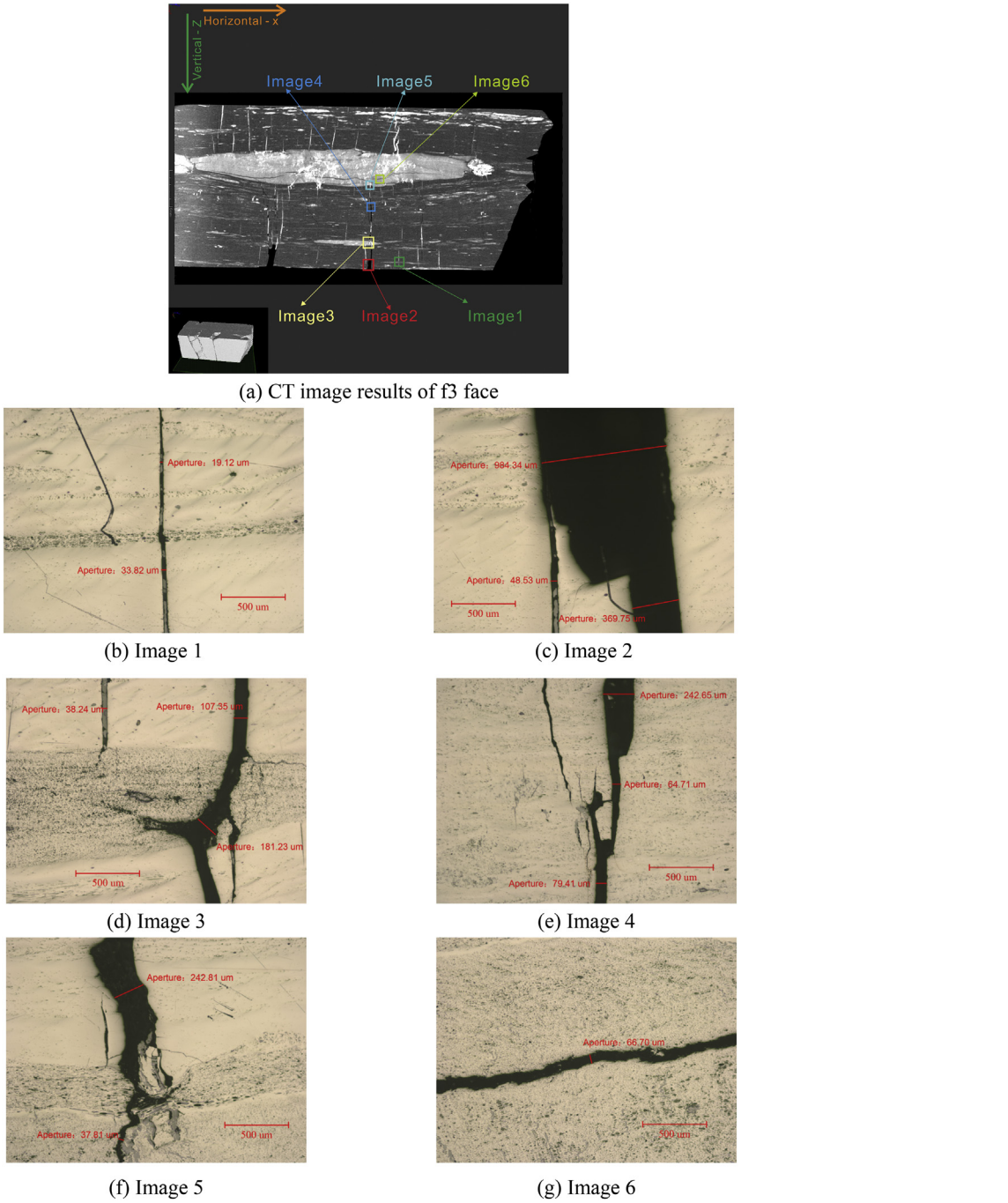

Fig. 5. Fracture distribution on the surface of face f3 of the coal sample as recovered through x-ray CT imaging (a) and optical microscopy (b-g).

equilibrating, pore pressure was gradually increased from 0 to 1.0 MPa, at a rate of 0.1 MPa/10s, and then remained constant at 1.0 MPa. The temperature was maintained at 26.5 ± 0.3 °C during the entire experiment.

3. Experimental results and discussion

The characterized samples are subject to dynamic experiments involving sorption and measuring the active generation of surface strains at a spectrum of relevant scales. The permeability of the matrix system is estimated to be in the nano-Darcy range, according to the MICP tests. These define the characteristic of the matrix system and the fracture system for later analysis. The distributed strain gauges directly observed the evolution of *average* matrix strain for the full extent of the sample that is covered by the strain gauge.

3.1. Description of natural fracture systems

Coal is conceptualized as a dual porosity/permeability system containing porous matrix surrounded by fractures. In this study, the cleat system, fractures, joints, and faults are all included in the fracture system (Shi et al., 2018). It is commonly assumed that Darcy flow is a result of flow in the fracture system and that the contribution of Darcy flow in the coal matrix can be neglected (Purl et al., 1991). Thus the bulk permeability of a coal sample is a function of the fracture system (Palmer, 2009; Pan and Connell, 2012; Ried et al., 1992). Therefore, the distribution of the fracture network determines the primary pathway to gas flow, but the connectivity of this fracture system is influenced by

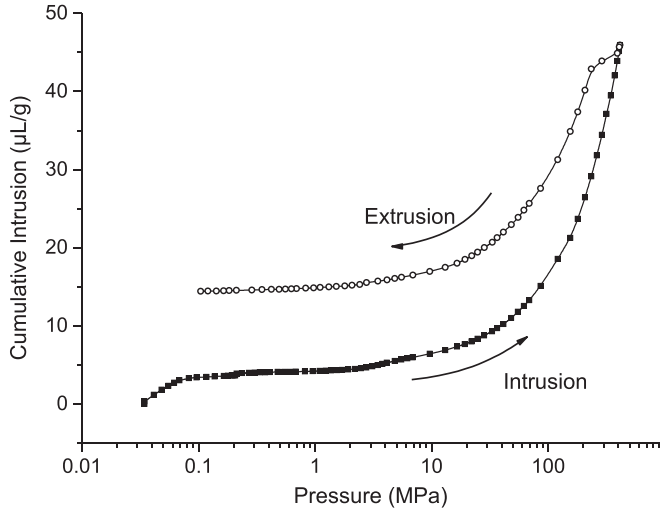

Fig. 6. Mercury intrusion and extrusion volumes with pressure for the coal sample.

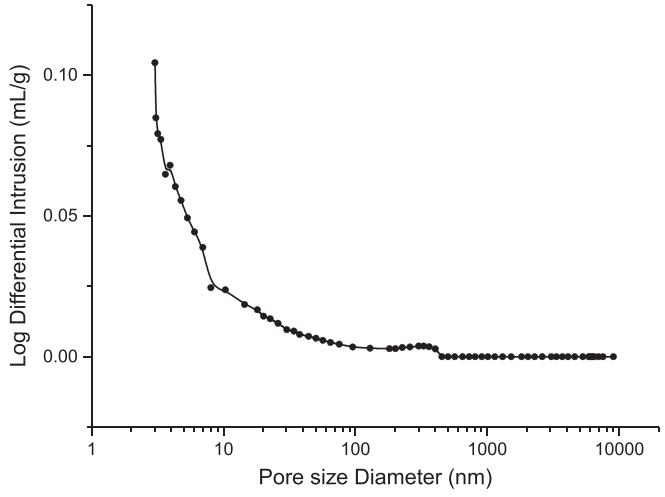

Fig. 7. Log differential intrusion volume vs. pore size diameter for the coal sample.

deformation of the matrix.

The distribution of fractures on face f2 is mostly in the Horizontal (−Y) direction, with most of these fractures filled with calcite (white lines), as shown in Fig. 4 (a). We selected two representative fractures for analysis – a small one and a large one. The small fractures show a largely uniform aperture which is of the order of ~8 μm within the field of view, as shown in image1 and image2 of Fig. 4 (b) and (c). Conversely, the single large fracture exhibits a relatively tortuous topology with a non-uniform aperture ranging from ~150 to ~850 μm within the field of view (see image3 and image4 in Fig. 4 (d) and (e)).

The distribution of fractures on face f3 is mostly in the Vertical-Z direction, with most of these fractures filled with calcite, as shown in Fig. 5 (a). The distribution of fractures on face f3 is more complex than that on face f2, as face f2 is perpendicular to bedding. Three representative fractures were selected for analysis. These are: (i) a small fracture as shown in image1 in Fig. 5 (b) which flanks the small fracture in Fig. 4 (b) and (c), (ii) a large fracture as shown in image2–5 in Fig. 5 (c-f) which flanks of the large fracture in Fig. 4 (d) and (e), and (iii) a fracture in a rock parting, as shown in image 6 in Fig. 5 (g).

3.2. Pore size distribution of matrix system from MICP tests

MICP is an effective tool in providing quantitative evaluation of pore structure. Fig. 6 shows the cumulative intrusion and extrusion volume versus the applied pressure for the studied coal sample. The pore size distribution is presented in Fig. 7. A significant volume of mercury intrudes the connected pores in the coal sample with an increase in applied pressure, suggesting that the sizes of some pores are in the meso-macropore range.

The average pore throat size, indexed by volume (50%) of the coal sample, is less than 10 nm. The permeabilities of the connected pore network for pore throat diameters (matrix system) in the range 4–10 nm is in nano-Darcy range (Hu et al., 2015; Katz and Thompson, 1986; Sun et al., 2017; Yang et al., 2017).

3.3. Changes of coal local linear strain with time

The fracture voids are devoid of filling and reject the attachment of the strain gauges – thus direct compression or extension cannot be measured on this section. The strain data acquired from the measurement is only able to evaluate the evolution of *average* matrix strain for the full extent of the sample that is covered by the strain gauge. Fig. 8 presents the evolution of the coal strains with time during injection of CH_4. Strain gauges A, B, C and D were located respectively on different parts of the sample face to sample the response of the different fracture distributions. Strain gauge A recorded the deformation of the overall sample; strain gauge B recorded the deformation of the part of the sample that crosses a large fracture; strain gauge C recorded the deformation of a small part of the sample that contains no fractures; and strain gauge D recorded the deformation of a small part of the sample that crosses a small fracture. The evolution of strains A and C with time can be divided into three stages, while the evolution of strains B and D with time can be classified into four stages. The monitoring results exhibit nearly the same trends. First, local linear strain increased rapidly from the initiation of gas injection (except for strain gauges A and C). Following that, the local linear strains begin to decrease gradually to reach a minimum, but the rate and magnitude of this decay was inconsistent. Subsequently, local linear strains begin to gradually increase and finally reach a plateau, with this process lasting for the extraordinarily extended period of two to three months. During this entire process, the maximum shrinkage strain was of the order of −292με, and the maximum swelling strain of about 1365με.

The deformation of different part of the sample with different fracture distributions show different evolutionary trends. Strain gauges A and B (black line and red line in Fig. 8), that cross large fractures and sample a relatively large tributary area of solid matrix, show nearly the same evolutionary trend. They reach nearly the same magnitude (about −100με) of maximum shrinkage strain and at the same time. Then these two local linear strains gradually increased and finally reached a plateau with a maximum swelling strain of ~1360με- but taking nearly three months to reach this equilibrium state. While for strain gauge D (cyan line in Fig. 8), which measures the deformation of a small part of the sample that crosses a small fracture, the evolutionary trend is totally different from that of strain gauges A and B. The maximum shrinkage strain is only approximately −9με, and it takes only slightly more than one month to reach the final plateau. For strain gauge C (blue line in Fig. 8), which measures the deformation of only a small part of the sample and that contains no fractures, the time taken to reach the final plateau is nearly the same as that for strain gauge D, but it shows a clear shrinkage displacement with a maximum shrinkage strain of approximately −292με.

These results show the different average matrix strain evolution rates and magnitudes for different parts of the sample. For the small strain gauges (C and D) close to the fracture, the equilibrium time is shorter than that for the larger gauges (A and B) measuring the response of a larger tributary area of the matrix that has no obvious fractures

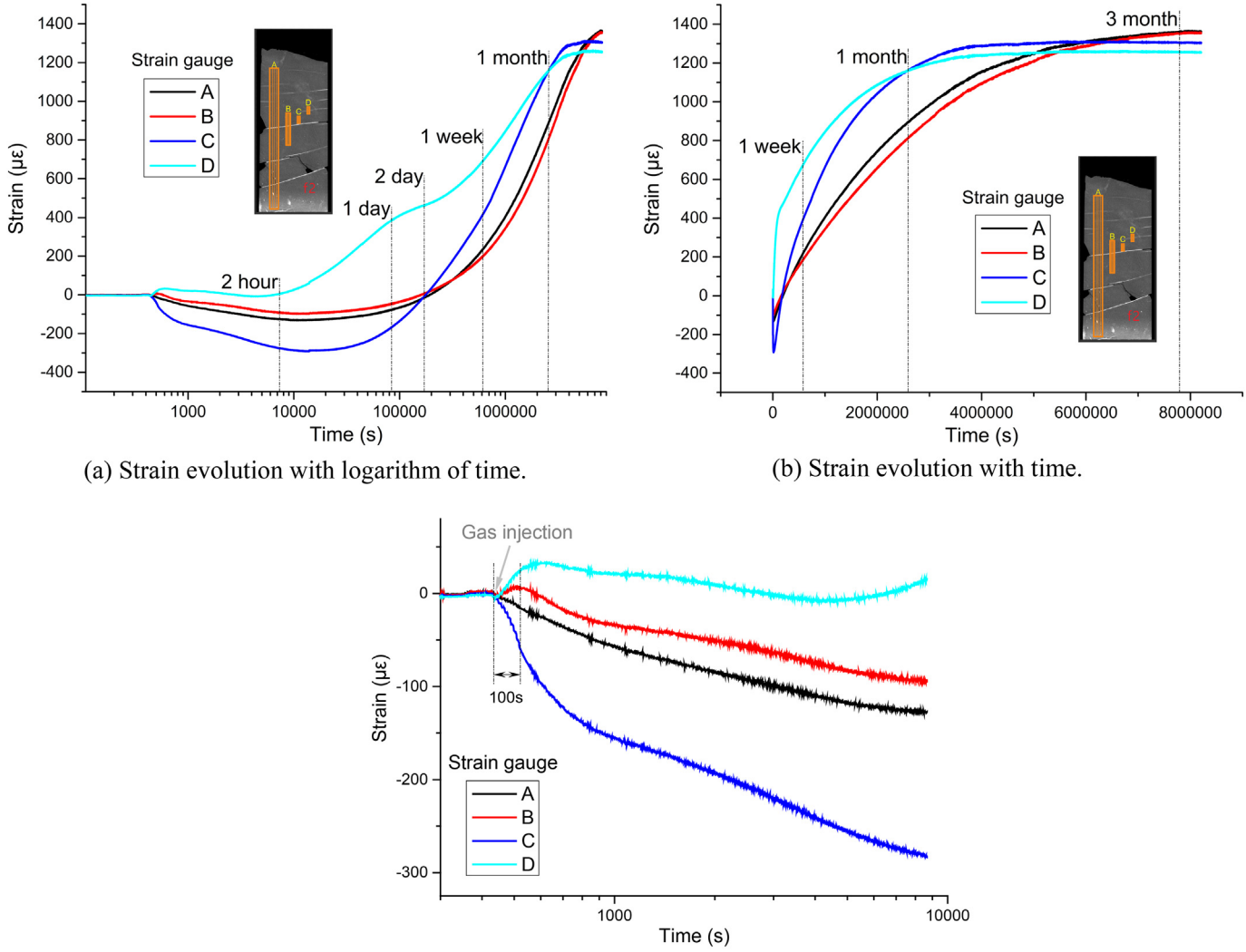

(a) Strain evolution with logarithm of time.

(b) Strain evolution with time.

(c) Strain evolution –with logarithm of time, in the first 2 hours.

Fig. 8. Evolution of strain with time during injection of CH_4.

present. It takes nearly two to three months to reach the final equilibrium state of this system, which is much longer than the typical "equilibrium time" used in experimental measurements of permeability. However, most significantly, the average matrix strains do not evolve monotonically throughout the experiment, which is generally assumed in most permeability models that do not accommodate this spatial evolution in deformation and strain – this is a fundamental observation that is important in correctly characterizing such systems. Thus, to further analyze these interaction mechanisms, we constructed a numerical model to analyze the experimental results.

4. Numerical model implementation and validation

In the following, a fully coupled numerical model is implemented to understand principal active mechanisms of sorption-induced straining and to reconcile laboratory observed response. Specifically, we match modeling results with laboratory measurements, to numerically simulate the spatial distribution of strain, to explore the dynamics of stress transfer between the matrix and the fracture, and to model the evolution of coal permeability from initial to ultimate equilibrium.

4.1. Governing equations of coal deformation

We assume that both the matrix and the fracture are homogeneous and elastic, and that deformation obeys Hooke's law. The deformation of a homogeneous, isotropic, and uniform elastic medium can be described by the Navier-type equation both in the matrix region and the fracture region (Wu et al., 2010):

$$Gu_{i,kk} + \frac{G}{1-2\nu}u_{k,ik} - \alpha p - K\varepsilon_L \frac{p_L}{(p+p_L)^2}p_i + f_i = 0 \quad (1)$$

where $G = E/2(1+\nu)$, $K = E/3(1-2\nu)$, G is the shear modulus, u_i is the component of displacement in the i-direction, ν is the Possion's ratio, α is the Biot's coefficient, K is the bulk modulus, E is the Young's modulus, ε_L is the Langmuir volumetric strain constant representing the volumetric strain at infinite pore pressure only in the matrix region, p_L is the Langmuir pressure at which the measured volumetric strain is equal to 0.5 ε_L only in the matrix region, p is the pore pressure, and f_i is the component of body force in the i –direction. Specifically, these parameters represent different properties (e.g., G_m is the shear modulus of the matrix, G_f is the shear modulus of the fracture) for the matrix and fracture.

4.2. Mass balance equation

The flow in both fracture and matrix is assumed to be governed by Darcy's law. Although it is commonly assumed that Darcy flow predominates in the fracture system, and diffusion may dominate in the

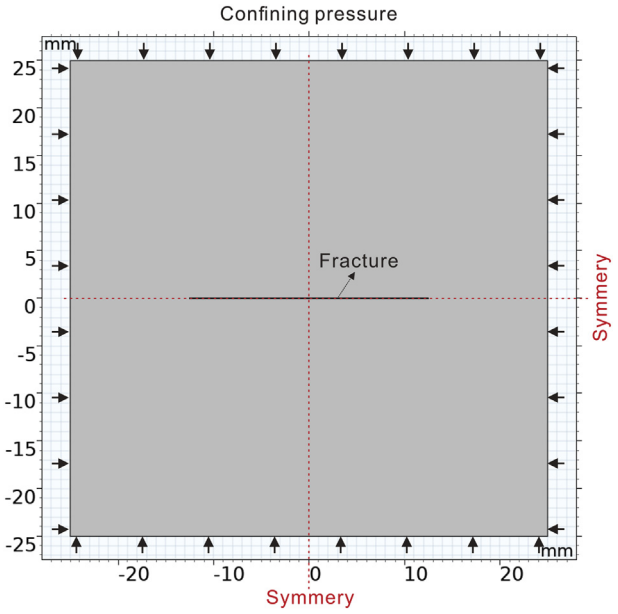

Fig. 9. Geometry of the 2D symmetric model together with boundary conditions.

coal matrix (Purl et al., 1991) – because there are equivalencies between permeability and diffusivity.

(1) Governing equation for gas flow within matrix.

According to our previous work (Wei et al., 2019a), for the case of an ideal absorbing gas, the governing equations for matrix and fracture are:

$$\frac{\mathrm{d}}{\mathrm{d}t}\left(\phi_m p_m \frac{\mathrm{M}}{\mathrm{RT}} + (1-\phi_m)\rho_s \rho_a \frac{V_L p_m}{p_m + P_L}\right) - \nabla\left(\rho_g \frac{k_m}{\mu}\nabla p_m\right) = Q_S \tag{2}$$

where ϕ_m is the porosity of matrix system, p_m is the gas pressure in the matrix, M is the molecular mass of gas, R is the universal gas constant, T is the absolute gas temperature, ρ_s is coal density, ρ_a is gas density at atmospheric pressure, V_L is the Langmuir volume constant, ρ_g is the gas density, μ is the dynamic viscosity of the gas, k_m is the permeability of matrix system, and Q_S is the gas source or sink.

(2) Governing equation for gas flow within fracture.

Gas transfer through the fractures is governed by the basic mass conservation relation of the fracture system, but is rarely used in models of matrix-fracture interaction, due to the rapid equilibration within the fracture (Liu et al., 2018). Thus, the pore pressure in the fracture p_f is assumed to be increased gradually within 100 s from the application of the initial pore pressure p_{m0} (0.1 MPa) to a constant p_1 (1.0 MPa).

$$p_f = \begin{cases} p_1 & t \geq 100s \\ t * 0.009 * p_1 + p_{m0} & t < 100s \end{cases} \tag{3}$$

The fracture permeability is defined by the well-known "cubic law" (Witherspoon et al., 1980) and the fracture permeability ratio can be expressed as:

$$\frac{k_f}{k_{f_0}} = \left(1 + \frac{\Delta b}{b_0}\right)^3 \tag{4}$$

where k_f is the fracture permeability, k_{f0} is the initial fracture permeability, b_0 is initial fracture aperture and Δb is the change in fracture aperture. The field equations are implemented and solved using COMSOL Multiphysics.

4.3. Model implementation and validation

As shown in Fig. 9, the sample is simplified as a 2D model with both length and height of 50 mm. A fracture is distributed in the middle of the sample (black line in Fig. 9), and the length of the fracture is 25 mm with an aperture of 45 μm. Injection of CH_4 is taken as an example to illustrate how mass and stress transfer between the matrix and the fracture are coupled under the constant confining pressure condition and the distribution of the heterogeneous strains inside the coal sample under the influence of gas-sorption determined. It is assumed that the gas is injected into the center of the model. No flow conditions are applied to all external boundaries with mass exchange between the matrix and fracture occurring on the connecting boundary. The interface boundary condition between the matrix and fracture domains is one of pressure continuity across interior boundary (Wei et al., 2019a). The mass transfer between the matrix and fracture is applied at the interface between these two systems. The applied confining pressure and pore pressure increase gradually within 100 s to a constant (1.0 MPa). Relevant initial values of parameters for fracture and matrix system in the simulation model are listed in Table 1. Simulated strain evolution in different part of the sample is compared with the experimental results at the same stress conditions in Fig. 10. Results show that the modeled evolution of strain is in good agreement with the strains that are directly measured by strain gauges A and C on the sample.

4.4. Analysis of pore pressure, stress and strain evolution

Fig. 11 shows the distribution of pore pressure, stress and strain in the matrix at different times during CH_4 injection. The correlation

Table 1
Property parameters of explicit model.

Parameters	Value	Source
Young's modulus of matrix, E_m	5.5 GPa	Modified according to Liu et al., 2018
Young's modulus of fracture, E_f	0.05 GPa	Modified according to Liu et al., 2018
Langmuir volume of matrix, V_L	0.017 m^3/kg	Modified according to Liu et al., 2018
Langmuir pressure of matrix, p_L	3 MPa	Modified according to Liu et al., 2018
Langmuir volumetric strain, ε_L	0.0093	Zhang et al., 2018
Possion's ratio of matrix, ν_m	0.35	Zhang et al., 2018
Possion's ratio of fracture, ν_f	0.35	Zhang et al., 2018
Biot's coefficient, α	0.7	Zhang et al., 2018
Coal density, ρ_s	1500 kg/m^3	Zhang et al., 2018
Viscosity of the gas, μ	1.84×10^{-5}	Constant
Porosity of matrix	0.02	Zhang et al., 2018
Permeability of matrix, k_m	2.3×10^{-21} m^2	Modified according to Wei et al., 2019b
Initial fracture aperture, b_0	45 μm	Experimental test
Injection pressure, p_1	1 MPa	Experimental setting

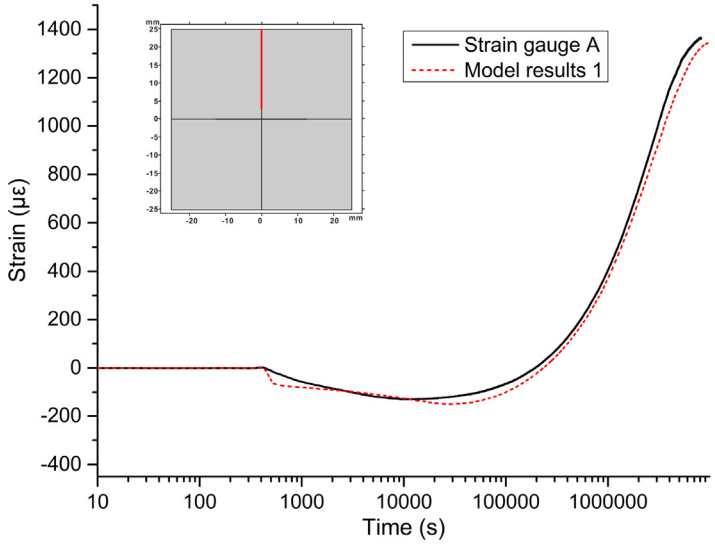

(a) Comparison between model and experimental results for strain gauge A.

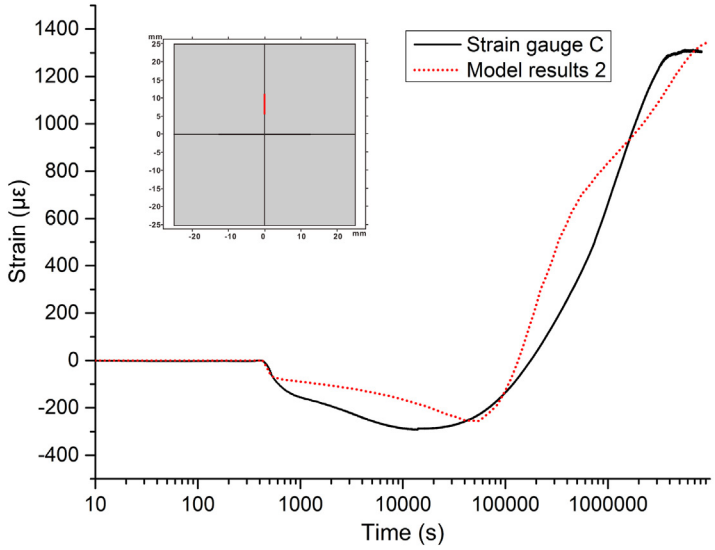

(b) Comparison between model and experimental results for strain gauge C.

Fig. 10. Comparison between the model results and experimental data.

between the evolution of strain (solid line) and pressure (dotted line) at the red line in the sample (model results 1 in Fig. 10 (a)) at different time is presented in Fig. 12.

Prior to injection, the sample is at equilibrium (pressure, stress and mass contents) and no disequilibrium interaction between the matrix and the fracture occurs (Fig. 11 (1) and Fig. 12 (initial state)). Post-injection, a series of processes initiate. Confining pressure and pore pressure are increased gradually from 0 to 1.0 MPa within 100 s, and then maintain constant at 1.0 MPa. First, gas rapidly invades the fracture due to its relatively high permeability, then the distribution of the gas pressure in the fracture remains constant, leading to a pressure difference between the matrix and the fracture (Fig. 11 (2) and Fig. 12). Next, with the gas contacting the fracture surface and diffusing into the matrix, local strains evolve in the matrix due to both the gas adsorption and the increasing gas pressure, which occurs only locally in the direct vicinity of the fracture. These coupled diffusion/sorption phenomena determine the localized deformation within the ensemble matrix-fracture system. Under this condition, the matrix near the fracture swells, causing the fracture to narrow/compact, and shrinkage of the matrix occurs far from the fracture due to the redistribution of stress (Fig. 11 (2) and Fig. 12 (2 h, 1 day)). As gas injection continues, the swelling zone widens as the gas diffuses further into the matrix of the sample (Fig. 11 (2–5)). The gas pressure front propagates throughout the matrix until a new equilibrium state between the fracture and the matrix is attained (Fig. 11 (6) and Fig. 12 (final equilibrium state)). The results show that during this non-equilibrium condition, the swelling of the matrix near the fracture will cause not only compaction and narrowing of the fracture, but also shrinkage of the matrix that is distant from the fracture. The above analysis demonstrates that many permeability measurements in ultra-low permeability rocks may have been conducted under the non-equilibrium conditions, suggesting that the interactions between the matrix and the fracture must be taken into

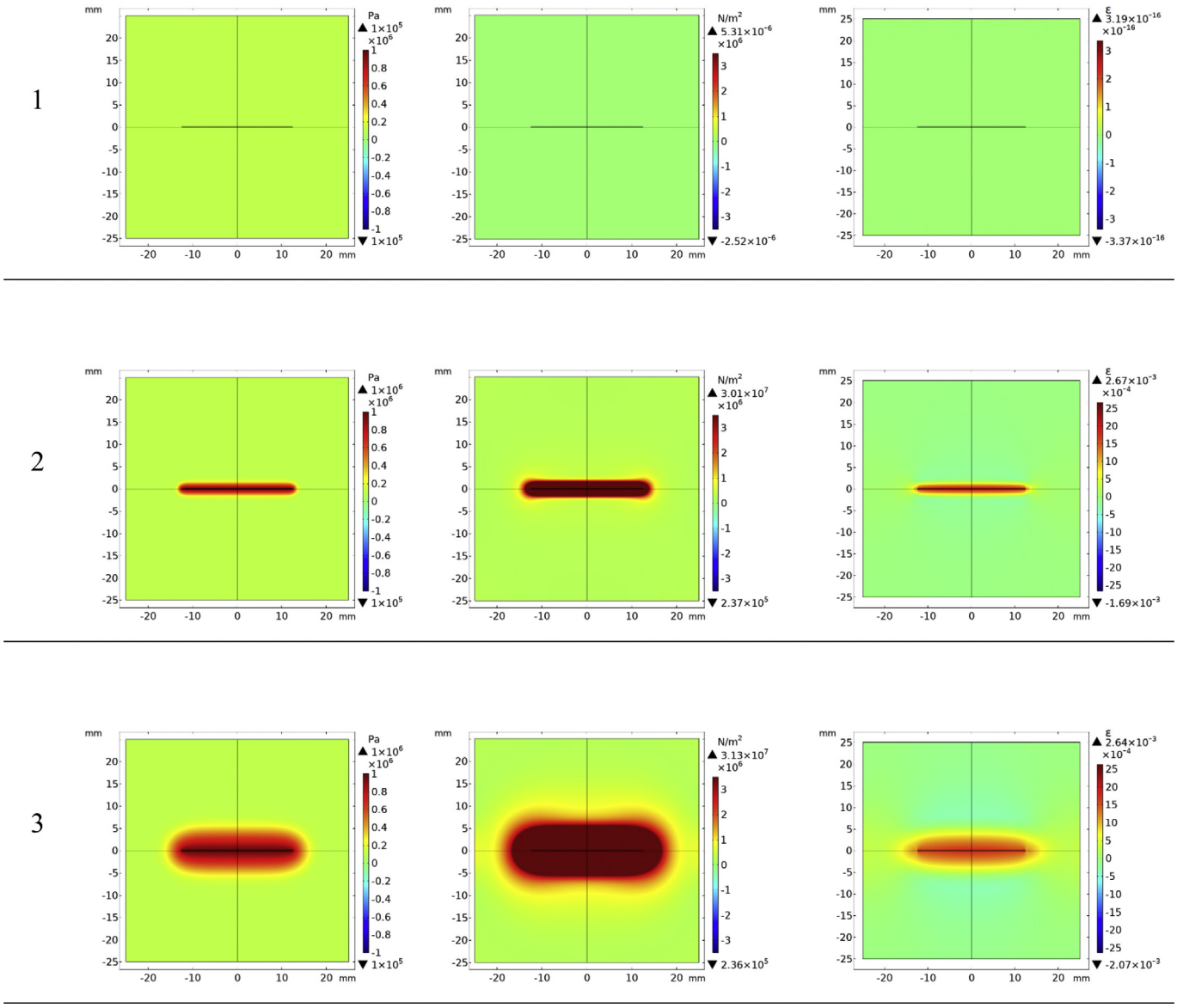

Fig. 11. Distribution of pore pressure, stress and strain in matrix at different times during CH_4 injection.

consideration to fully understand the stress transfers and to correctly interpret the permeability evolution. This indicates a significant gap between most of the existing equilibrium-assumption permeability models and laboratory experiments.

4.5. Analysis of permeability evolution

In the prior experimental and numerical observations of ultra-low permeability coal, strains are demonstrated to change throughout the entire period of experiment and in turn alter the fracture aperture-determining the evolution of non-equilibrium facture permeability.

Fig. 13 shows the evolution of permeability based on our model. The behavior can be divided into three stages under our particular experimental conditions: (1) Stage 1 - permeability decrease. During the gas injection period, the applied confining pressure and pore pressure increase gradually from 0 to 1.0 MPa within 100 s and then remain constant at 1.0 MPa. There is an aperture reduction induced by the influence of Biot's coefficient and a time delay for the equilibration of pore pressure both in the fracture system and the matrix system. As the gas diffuses from fracture to matrix, the gas pressure in the matrix slowly increases. This process leads to the swelling of the matrix adjacent to the fracture (Fig. 11 (2–3) and Fig. 12 (2 h, 1 day)). In addition, this localization of swelling reduces the fracture aperture and further causes a decrease of permeability; (2) Stage 2 - permeability recovery. As the gas front propagates from the vicinity of the fracture wall to the exterior region (distant from the fracture), the matrix strain becomes more uniform (Fig. 11 (4–5) and Fig. 12 (1 week, 2 weeks)). At this stage, the effect of local strain in the matrix vanishes with the permeability beginning to gradually increase and finally reaching a plateau, which lasts for the extraordinarily extended period of three

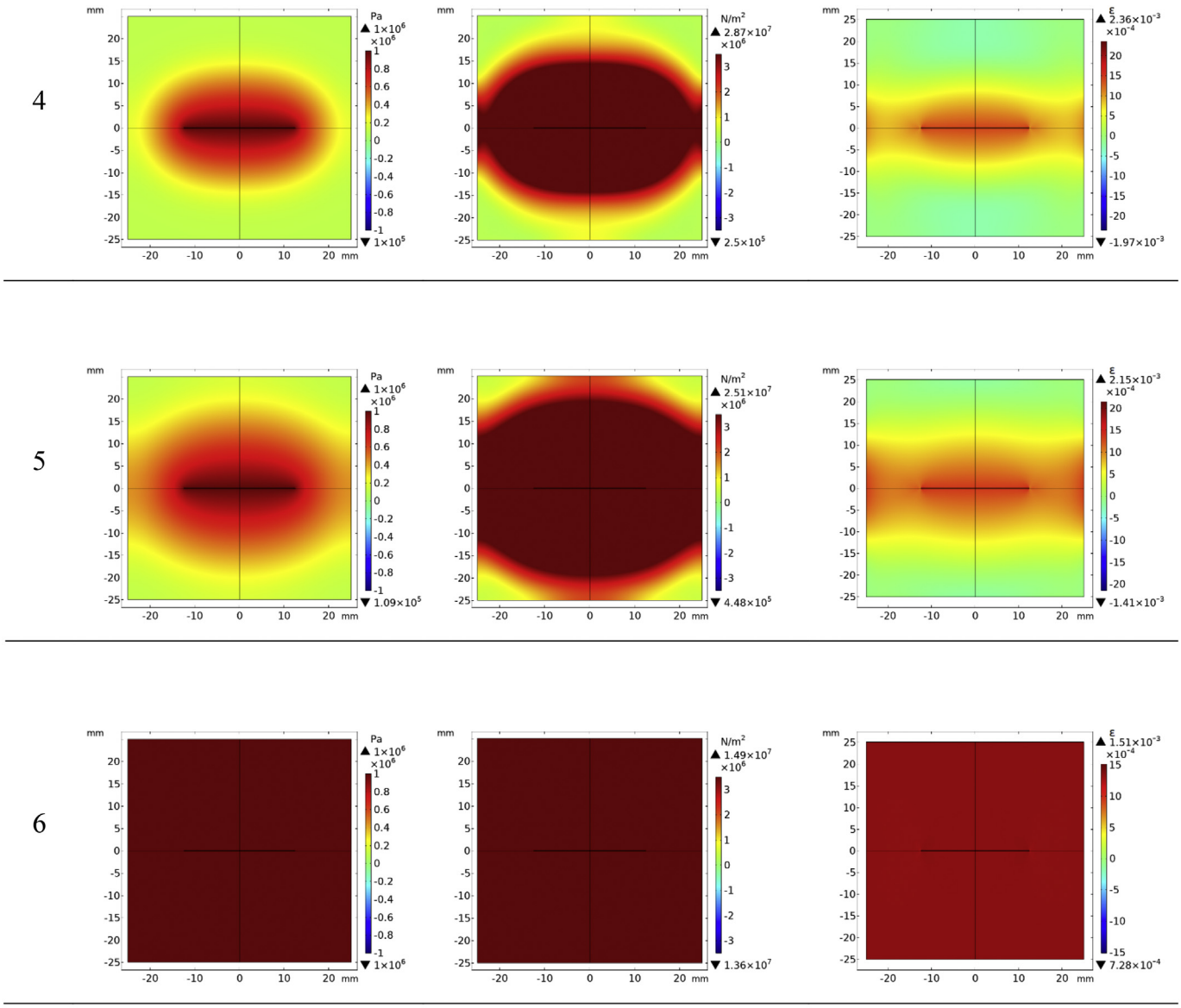

(1) Initial state - before gas injection; (2) 2 hour - after gas injection; (3) 1 day - after gas injection; (4) 1 week - after gas injection; (5) 2 week - after gas injection; (6) Final equilibrium state.

Fig. 11. (*continued*)

months; (3) Stage 3 - permeability stabilization. When a final equilibrium state is reached, the effect of local strain completely vanishes (Fig. 11 (6) and Fig. 12 (final equilibrium state)) and the permeability remains unchanged. Thus, permeability changes during non-equilibrium states are the consequences of complex interactions between coal matrix and fracture. Similar process will also prevail during gas extraction (e.g., coalbed methane production, shale gas extraction) rather than injection, which is studied here.

5. Conclusions

In this study, we directly measured and analyzed the strain evolution of a prismatic coal sample during gas injection to experimentally determine how coal strain/permeability evolves from initial to ultimate equilibrium. The following conclusions can be drawn:

- The experimental results show that the interval from initial to final equilibrium is much longer than that generally assumed and reported in the literature. The final equilibrium state (pressure, stress and mass contents) for the matrix system may take an unusually long time and therefore the current permeability measurements may reflect non-equilibrium permeability evolutions. Although the disequilibrium sorbing masses are potentially small, the innate sensitivity of permeability in the matrix-fracture system makes permeability estimates potentially quite sensitive to this disequilibrium state.
- During the non-equilibrium condition, the distribution of deformations in different parts of the sample is not uniformly distributed in space or in time – rather they are strongly related to the fracture geometry and related gas saturation conditions. The swelling of the matrix near the fracture will cause not only compaction and narrowing of the fracture, but also shrinkage of the matrix that is

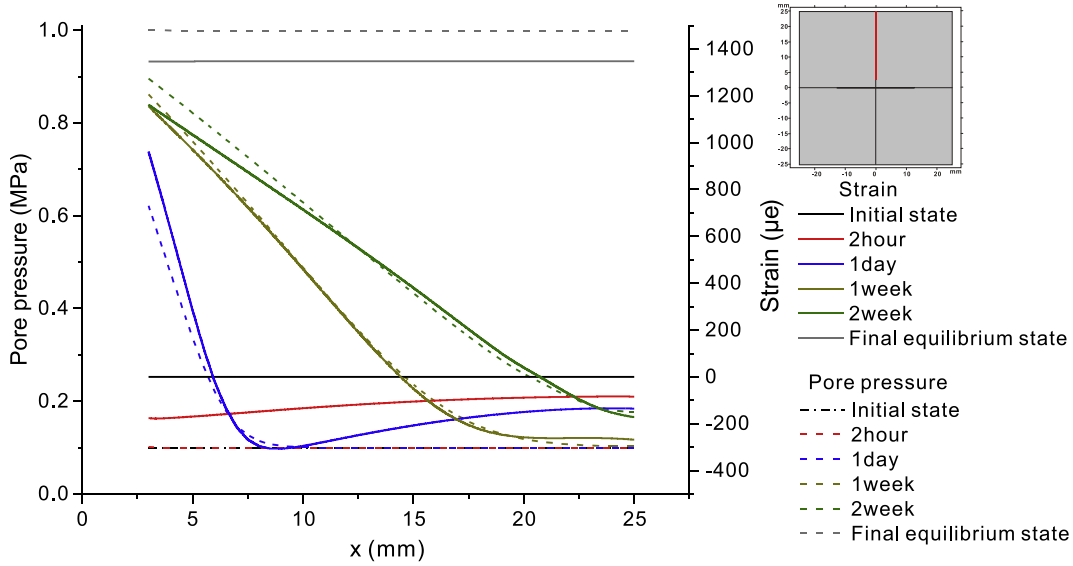

Fig. 12. Correlation between gas pressure and strain evolution.

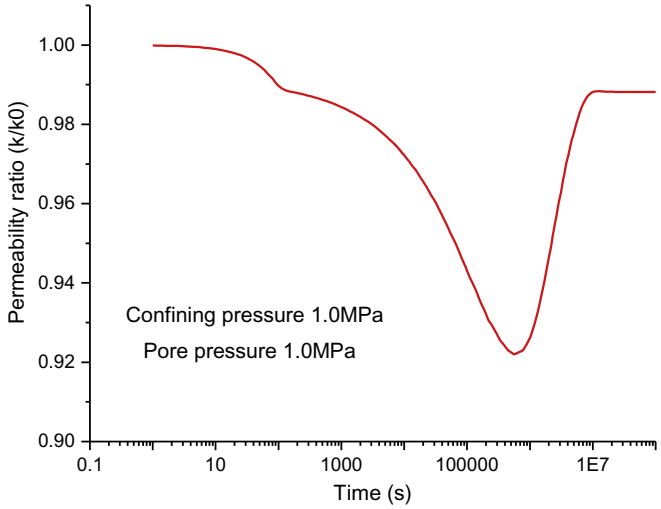

Fig. 13. Evolution of fracture permeability ratio.

distant from the fracture under constant confining pressure condition.

- Coal strains change through the entire duration of the experiment and in turn alter the fracture aperture, with the evolution of non-equilibrium strain/permeability determined by the matrix-fracture interactions while that of equilibrium permeability is defined by the overall behavior.
- There is a gap between most of the existing equilibrium-assumption permeability models and laboratory experiments. This gap is determined mainly by a lack of recognition of this prominent non-equilibrium state and the impact of matrix-fracture interactions including sorption-induced swelling/shrinking for all gas pressures. Permeability changes through this non-equilibrium state are the consequence of complex interactions between coal matrix and fracture and may be much more common and of much longer duration than previously suspected.

Declaration of Competing Interest

The authors declare that they have no conflict of interest.

Acknowledgments

This work was funded by the Natural Science Foundation of China, China (41972184), the Fund of Outstanding Talents in Discipline of China University of Geosciences (Wuhan) (102-162301192664), and the Fundamental Research Funds for National Universities, China University of Geosciences (Wuhan). Those sources of support are gratefully acknowledged.

References

Al-hawaree, M., 1999. Geomechanics of CO2 Sequestration in Coalbed Methane Reservoirs. University of Alberta.
Anggara, F., Sasaki, K., Sugai, Y., 2016. The correlation between coal swelling and permeability during CO 2 sequestration: a case study using Kushiro low rank coals. Int. J. Coal Geol. 166, 62–70.
Bai, M., Elsworth, D., Roegiers, J.C., 1993. Multiporosity/multipermeability approach to the simulation of naturally fractured reservoirs. Water Resour. Res. 29, 1621–1633.
Chen, Z., Pan, Z., Liu, J., Connell, L.D., Elsworth, D., 2011. Effect of the effective stress coefficient and sorption-induced strain on the evolution of coal permeability: experimental observations. Int. J. Greenh. Gas Control. 5, 1284–1293.
Connell, L.D., Lu, M., Pan, Z., 2010. An analytical coal permeability model for tri-axial strain and stress conditions. Int. J. Coal Geol. 84, 103–114.
Cui, X., Bustin, R.M., 2005. Volumetric strain associated with methane desorption and its impact on coalbed gas production from deep coal seams. AAPG Bull. 89, 1181–1202.
Cui, G., Liu, J., Wei, M., Feng, X., Elsworth, D., 2018a. Evolution of permeability during the process of shale gas extraction. J. Nat. Gas Sci. Eng. 49, 94–109.
Cui, G., Liu, J., Wei, M., Shi, R., Elsworth, D., 2018b. Why shale permeability changes under variable effective stresses: new insights. Fuel. 213, 55–71.
Danesh, N.N., Chen, Z., Connell, L.D., Kizil, M.S., Pan, Z., Aminossadati, S.M., 2017. Characterisation of creep in coal and its impact on permeability: an experimental study. Int. J. Coal Geol. 173, 200–211.
Fan, L., Liu, S., 2018. Numerical prediction of in situ horizontal stress evolution in coalbed methane reservoirs by considering both poroelastic and sorption induced strain effects. Int. J. Rock Mech. Min. Sci. 104, 156–164.
Fan, C., Elsworth, D., Li, S., Zhou, L., Yang, Z., Song, Y., 2019. Thermo-hydro-mechanical-chemical couplings controlling CH4 production and CO2 sequestration in enhanced coalbed methane recovery. Energy. 173, 1054–1077.
Feng, R., Harpalani, S., Pandey, R., 2017. Evaluation of various pulse-decay laboratory permeability measurement techniques for highly stressed coals. Rock Mech. Rock. Eng. 50, 297–308.
Gan, H., Nandi, S., Walker Jr., P., 1972. Nature of the porosity in American coals. Fuel. 51, 272–277.
Gensterblum, Y., Ghanizadeh, A., Krooss, B.M., 2014. Gas permeability measurements on Australian subbituminous coals: fluid dynamic and poroelastic aspects. J. Nat. Gas Sci. Eng. 19, 202–214.
Guo, R., Mannhardt, K., Kantzas, A., 2007. Laboratory Investigation on the Permeability of Coal during Primary and Enhanced Coalbed Methane Production. Canadian International Petroleum Conference, Calgary, pp. 1–8.
Haenel, M.W., 1992. Recent progress in coal structure research. Fuel. 71, 1211–1223.
Harpalani, S., Chen, G., 1995. Estimation of changes in fracture porosity of coal with gas emission. Fuel. 74, 1491–1498.
Harpalani, S., Chen, G., 1997. Influence of gas production induced volumetric strain on permeability of coal. Geotech. Geol. Eng. 15, 303–325.

Harpalani, S., Schraufnagel, R.A., 1989. Flow of Methane in Deep Coal Seams. ISRM International Symposium, Pau, pp. 195–201.
Harpalani, S., Schraufnagel, R.A., 1990. Shrinkage of coal matrix with release of gas and its impact on permeability of coal. Fuel. 69, 551–556.
Harpalani, S., Zhao, X., 1989. The unusual response of coal permeability to varying gas pressure and effective stress. In: the 30th US Symposium on Rock Mechanics (USRMS), pp. 65–72 Morgantown.
Hu, Q., Ewing, R.P., Rowe, H.D., 2015. Low nanopore connectivity limits gas production in Barnett formation. J. Geophys. Res. 120, 8073–8087.
Izadi, G., Wang, S., Elsworth, D., Liu, J., Wu, Y., Pone, D., 2011. Permeability evolution of fluid-infiltrated coal containing discrete fractures. Int. J. Coal Geol. 85, 202–211.
Karacan, C.Ö., 2007. Swelling-induced volumetric strains internal to a stressed coal associated with CO2 sorption. Int. J. Coal Geol. 72, 209–220.
Karacan, C.Ö., Ruiz, F.A., Cotè, M., Phipps, S., 2011. Coal mine methane: a review of capture and utilization practices with benefits to mining safety and to greenhouse gas reduction. Int. J. Coal Geol. 86, 121–156.
Katz, A., Thompson, A., 1986. Quantitative prediction of permeability in porous rock. Phys. Rev. B 34, 8179.
Kiyama, T., Nishimoto, S., Fujioka, M., Xue, Z., Ishijima, Y., Pan, Z., Connell, L.D., 2011. Coal swelling strain and permeability change with injecting liquid/supercritical CO2 and N2 at stress-constrained conditions. Int. J. Coal Geol. 85, 56–64.
Kumar, H., Elsworth, D., Liu, J., Pone, D., Mathews, J.P., 2012. Optimizing enhanced coalbed methane recovery for unhindered production and CO 2 injectivity. Int. J. Greenh. Gas Control. 11, 86–97.
Li, J., Liu, D., Yao, Y., Cai, Y., Chen, Y., 2013. Evaluation and modeling of gas permeability changes in anthracite coals. Fuel. 111, 606–612.
Li, J., Liu, D., Lu, S., Yao, Y., Xue, H., 2015. Evaluation and modeling of the CO2 permeability variation by coupling effective pore size evolution in anthracite coal. Energy Fuel 29, 717–723.
Lin, W., Kovscek, A.R., 2014. Gas sorption and the consequent volumetric and permeability change of coal I: experimental. Transp. Porous Media 105, 371–389.
Lin, W., Tang, G.-Q., Kovscek, A.R., 2008. Sorption-induced permeability change of coal during gas-injection processes. SPE Reserv. Eval. Eng. 11, 792–802.
Liu, S., Harpalani, S., 2013. A new theoretical approach to model sorption-induced coal shrinkage or swelling. AAPG Bull. 97, 1033–1049.
Liu, J., Chen, Z., Elsworth, D., Miao, X., Mao, X., 2011a. Evolution of coal permeability from stress-controlled to displacement-controlled swelling conditions. Fuel. 90, 2987–2997.
Liu, J., Chen, Z., Elsworth, D., Qu, H., Chen, D., 2011b. Interactions of multiple processes during CBM extraction: a critical review. Int. J. Coal Geol. 87, 175–189.
Liu, Q., Cheng, Y., Ren, T., Jing, H., Tu, Q., Dong, J., 2016a. Experimental observations of matrix swelling area propagation on permeability evolution using natural and reconstituted samples. J. Nat. Gas Sci. Eng. 34, 680–688.
Liu, S., Wang, Y., Harpalani, S., 2016b. Anisotropy characteristics of coal shrinkage/swelling and its impact on coal permeability evolution with CO2 injection. Greenh. Gases Sci. Technol. 6, 615–632.
Liu, T., Lin, B., Yang, W., 2017. Impact of matrix–fracture interactions on coal permeability: model development and analysis. Fuel. 207, 522–532.
Liu, X., Sheng, J., Liu, J., Hu, Y., 2018. Evolution of coal permeability during gas injection - from initial to ultimate equilibrium. Energies. 11, 2800.
Liu, Y., Yin, G., Li, M., Zhang, D., Deng, B., Liu, C., Lu, J., 2019. Anisotropic mechanical properties and the permeability evolution of cubic coal under true triaxial stress paths. Rock Mech. Rock. Eng. 1–17.
Lu, M., Connell, L.D., 2007. A model for the flow of gas mixtures in adsorption dominated dual porosity reservoirs incorporating multi-component matrix diffusion: part I. Theor. Dev. J. Pet. Sci. Eng. 59, 17–26.
Lu, M., Connell, L.D., 2011. A statistical representation of the matrix–fracture transfer function for porous media. Transp. Porous Media 86, 777–803.
Ma, Q., Harpalani, S., Liu, S., 2011. A simplified permeability model for coalbed methane reservoirs based on matchstick strain and constant volume theory. Int. J. Coal Geol. 85, 43–48.
Mazumder, S., Wolf, K.H., 2008. Differential swelling and permeability change of coal in response to CO 2 injection for ECBM. Int. J. Coal Geol. 74, 123–138.
McKee, C.R., Bumb, A.C., Koenig, R.A., 1988. Stress-dependent permeability and porosity of coal and other geologic formations. SPE Form. Eval. 3, 81–91.
Meng, Y., Li, Z., 2017. Triaxial experiments on adsorption deformation and permeability of different sorbing gases in anthracite coal. J. Nat. Gas Sci. Eng. 46, 59–70.
Meng, J., Nie, B., Zhao, B., Ma, Y., 2015. Study on law of raw coal seepage during loading process at different gas pressures. Mining Science and Technology (China). 25, 31–35.
Mitra, A., Harpalani, S., Liu, S., 2012. Laboratory measurement and modeling of coal permeability with continued methane production: part 1-Laboratory results. Fuel. 94, 110–116.
Palmer, I., 2009. Permeability changes in coal: analytical modeling. Int. J. Coal Geol. 77, 119–126.
Palmer, I., Mansoori, J., 1996. How Permeability Depends on Stress and Pore Pressure in Coalbeds: A New Model. (SPE Annual Technical Conference and Exhibition).
Pan, Z., Connell, L.D., 2007. A theoretical model for gas adsorption-induced coal swelling. Int. J. Coal Geol. 69, 243–252.
Pan, Z., Connell, L.D., 2012. Modelling permeability for coal reservoirs: a review of analytical models and testing data. Int. J. Coal Geol. 92, 1–44.
Pan, Z., Connell, L.D., Camilleri, M., 2010. Laboratory characterisation of coal reservoir permeability for primary and enhanced coalbed methane recovery. Int. J. Coal Geol. 82, 252–261.
Peng, Y., Liu, J., Wei, M., Pan, Z., Connell, L.D., 2014. Why coal permeability changes under free swellings: new insights. Int. J. Coal Geol. 133, 35–46.
Pini, R., Ottiger, S., Burlini, L., Storti, G., Mazzotti, M., 2009. Role of adsorption and swelling on the dynamics of gas injection in coal. J. Geophys. Res. 114.
Purl, R., Evanoff, J., Brugler, M., 1991. Measurement of coal cleat porosity and relative permeability characteristics. In: SPE Gas Technol. Symp. Houston, pp. 93–104.
Ried, G., Towler, B., Harris, H., 1992. Simulation and economics of coalbed methane production in the powder river basin. In: SPE Rocky Mountain Regional Meeting. Casper, pp. 425–432.
Robertson, E.P., Christiansen, R.L., 2005. Modeling Permeability In Coal Using Sorption-Induced Strain Data. Idaho National Laboratory (INL).
Robertson, E.P., Christiansen, R.L., 2006. A Permeability Model For Coal And Other Fractured, Sorptive-Elastic Media. Idaho National Laboratory (INL).
Sang, G., Elsworth, D., Liu, S., Harpalani, S., 2017. Characterization of swelling modulus and effective stress coefficient accommodating sorption-induced swelling in coal. Energy Fuel 31, 8843–8851.
Seidle, J.R., Huitt, L., 1995. Experimental measurement of coal matrix shrinkage due to gas desorption and implications for cleat permeability increases. In: International meeting on petroleum Engineering, pp. 575–582 Beijing.
Seidle, J., Jeansonne, M., Erickson, D., 1992. Application of matchstick geometry to stress dependent permeability in coals. In: SPE Rocky Mountain Regional Meeting. Casper, pp. 433–444.
Seomoon, H., Lee, M., Sung, W., 2015. Analysis of sorption-induced permeability reduction considering gas diffusion phenomenon in coal seam reservoir. Transp. Porous Media 108, 713–729.
Shi, J., Durucan, S., 2004. Drawdown induced changes in permeability of coalbeds: a new interpretation of the reservoir response to primary recovery. Transp. Porous Media 56, 1–16.
Shi, R., Liu, J., Wei, M., Elsworth, D., Wang, X., 2018. Mechanistic analysis of coal permeability evolution data under stress-controlled conditions. Int. J. Rock Mech. Min. Sci. 110, 36–47.
Siriwardane, H., Haljasmaa, I., McLendon, R., Irdi, G., Soong, Y., Bromhal, G., 2009. Influence of carbon dioxide on coal permeability determined by pressure transient methods. Int. J. Coal Geol. 77, 109–118.
Sun, M., Yu, B., Hu, Q., Yang, R., Zhang, Y., Li, B., 2017. Pore connectivity and tracer migration of typical shales in South China. Fuel. 203, 32–46.
Wang, S., Elsworth, D., Liu, J., 2011. Permeability evolution in fractured coal: the roles of fracture geometry and water-content. Int. J. Coal Geol. 87, 13–25.
Wang, J., Liu, J., Kabir, A., 2013. Combined effects of directional compaction, non-Darcy flow and anisotropic swelling on coal seam gas extraction. Int. J. Coal Geol. 109, 1–14.
Wang, Y., Liu, S., Elsworth, D., 2015. Laboratory investigations of gas flow behaviors in tight anthracite and evaluation of different pulse-decay methods on permeability estimation. Int. J. Coal Geol. 149, 118–128.
Wang, C., Liu, J., Feng, J., Wei, M., Wang, C., Jiang, Y., 2016. Effects of gas diffusion from fractures to coal matrix on the evolution of coal strains: experimental observations. Int. J. Coal Geol. 162, 74–84.
Wang, C., Zhai, P., Chen, Z., Liu, J., Wang, L., Xie, J., 2017a. Experimental study of coal matrix-cleat interaction under constant volume boundary condition. Int. J. Coal Geol. 181, 124–132.
Wang, K., Du, F., Wang, G., 2017b. Investigation of gas pressure and temperature effects on the permeability and steady-state time of chinese anthracite coal: an experimental study. J. Nat. Gas Sci. Eng. 40, 179–188.
Wang, L., Chen, Z., Wang, C., Elsworth, D., Liu, W., 2019. Reassessment of coal permeability evolution using steady-state flow methods: the role of flow regime transition. Int. J. Coal Geol. 103210.
Washburn, E.W., 1921. The dynamics of capillary flow. Phys. Rev. 17, 273.
Wei, M., Liu, J., Elsworth, D., Li, S., Zhou, F., 2019a. Influence of gas adsorption induced non-uniform deformation on the evolution of coal permeability. Int. J. Rock Mech. Min. Sci. 114, 71–78.
Wei, M., Liu, J., Shi, R., Elsworth, D., Liu, Z., 2019b. Long-term evolution of coal permeability under effective stresses gap between matrix and fracture during CO 2 injection. Transp. Porous Media 1–15.
Wei, M., Liu, Y., Liu, J., Elsworth, D., Zhou, F., 2019c. Micro-scale investigation on coupling of gas diffusion and mechanical deformation of shale. J. Pet. Sci. Eng. 175, 961–970.
Wildenschild, D., Sheppard, A.P., 2013. X-ray imaging and analysis techniques for quantifying pore-scale structure and processes in subsurface porous medium systems. Adv. Water Resour. 51, 217–246.
Witherspoon, P.A., Wang, J.S.Y., Iwai, K., Gale, J.E., 1980. Validity of cubic law for fluid flow in a deformable rock fracture. Water Resour. Res. 16, 1016–1024.
Wu, Y., Liu, J., Elsworth, D., Chen, Z., Connell, L., Pan, Z., 2010. Dual poroelastic response of a coal seam to CO2 injection. Int. J. Greenh. Gas Control. 4, 668–678.
Wu, Y., Liu, J., Chen, Z., Elsworth, D., Pone, D., 2011. A dual poroelastic model for CO2-enhanced coalbed methane recovery. Int. J. Coal Geol. 86, 177–189.
Xu, J., Cao, J., Li, B., Zhou, T., Minghui, L., Dong, L., 2013. Experimental research on response law of permeability of coal to pore pressure. Chin. J. Rock Mech. Eng. 32, 225–230.
Yang, Y., Liu, S., 2019. Estimation and modeling of pressure-dependent gas diffusion coefficient for coal: a fractal theory-based approach. Fuel. 253, 588–606.
Yang, R., Hao, F., He, S., He, C., Guo, X., Yi, J., Hu, H., Zhang, S., Hu, Q., 2017. Experimental investigations on the geometry and connectivity of pore space in organic-rich Wufeng and Longmaxi shales. Mar. Pet. Geol. 84, 225–242.
Zhang, S., Liu, J., Wei, M., Elsworth, D., 2018. Coal permeability maps under the influence of multiple coupled processes. Int. J. Coal Geol. 187, 71–82.
Zhang, Z., Zhang, R., Wu, S., Deng, J., Zhang, Z., Xie, J., 2019. The stress sensitivity and porosity sensitivity of coal permeability at different depths: a case study in the Pingdingshan mining area. Rock Mech. Rock. Eng. 52, 1539–1563.
Zhao, W., Cheng, Y., Pan, Z., Wang, K., Liu, S., 2019. Gas diffusion in coal particles: a review of mathematical models and their applications. Fuel. 252, 77–100.
Zheng, S., Yao, Y., Liu, D., Cai, Y., Liu, Y., 2018. Characterizations of full-scale pore size distribution, porosity and permeability of coals: a novel methodology by nuclear magnetic resonance and fractal analysis theory. Int. J. Coal Geol. 196, 148–158.